Anthropogenic impact on the severity of compound extreme high temperature and drought/rainy events in China

Bo Sun (sunb@nuist.edu.cn)
Collaborative Innovation Center on Forecast and Evaluation of Meteorological Disasters/Key Laboratory of Meteorological Disasters, Ministry of Education/Joint International Research Laboratory of Cl

Wanling Li
Nanjing University of Information Science and Technology https://orcid.org/0000-0002-0248-1755

Huijun Wang
Collaborative Innovation Center on Forecast and Evaluation of Meteorological Disasters/Key Laboratory of Meteorological Disasters, Ministry of Education/Joint International Research Laboratory of Cl

Botao Zhou
National Climate Center, China Meteorological Administration https://orcid.org/0000-0002-5995-2378

Huixin Li
Collaborative Innovation Center on Forecast and Evaluation of Meteorological Disasters/Key Laboratory of Meteorological Disasters, Ministry of Education/Joint International Research Laboratory of Cl

Rufan Xue
Collaborative Innovation Center on Forecast and Evaluation of Meteorological Disasters/Key Laboratory of Meteorological Disasters, Ministry of Education/Joint International Research Laboratory of Cl

Mingkeng Duan
Collaborative Innovation Center on Forecast and Evaluation of Meteorological Disasters/Key Laboratory of Meteorological Disasters, Ministry of Education/Joint International Research Laboratory of Cl

Xiaochun Luo
Meteorological Service Center of Jiangsu Province, Nanjing, China

Wenwen Ai
Meteorological Service Center of Jiangsu Province, Nanjing, China

Article

Keywords: Compound extreme events, Detection and attribution, Anthropogenic activities, Greenhouse gas forcing, Natural forcing

Posted Date: January 5th, 2023

DOI: https://doi.org/10.21203/rs.3.rs-2366543/v1

Abstract

Extreme events seriously affect human health and natural environment. In the present study, several indexes that can describe the severity of compound extreme high temperature and drought/rainy events (CHTDE/CHTRE) are constructed based on copulas. According to observations, CHTDE and CHTRE have intensified in most areas of China during 1961–2014. The significant increase trend in the severity of CHTDE and CHTRE is basically consistent with simulations under historical anthropogenic forcing. This result proves that changes in CHTDE can be largely attributed to anthropogenic climate change. The historical greenhouse gas forcing is identified to be the dominant factor that affects the severity of CHTDE in China, particularly in the Tibetan Plateau and Northwest China. Moreover, the contribution of anthropogenic forcing to the linear change of the CHTRE severity in China is more than 90%. In addition, the ozone and land use signals also can be detected on change of CHTDE and CHTRE.

Introduction

In recent years, as the global temperature continues to rise, extreme events such as extreme precipitation, extreme droughts, extreme high temperature and extreme storms occur frequently, causing devastating effects and risks to human life and ecological environment in various places[1–4]. For example, 38.305 million people were affected by the extreme high temperature event in China during the summer of 2022 (https://www.mem.gov.cn/xw/yjglbgzdt/202209/t20220917_422674.shtml). In the summer of 2021, China experienced many extreme rainfall events, each of which caused a property loss of about US$12 billion[5]. Furthermore, the Lancet Countdown Regional Centre in Asia reported that hundreds to thousands of people lost their lives in extreme floods each year in China, and millions to tens of millions of people cannot have drinking water because of extreme droughts[6]. In particular, in the context of global warming, compound extreme weather and climate events, which are multivariate extremes at multiple temporal and spatial scales that can further exacerbate the risks and effects caused by individual extreme events, become more frequent. The compound extreme events pose a serious threaten to communities and have great impacts on crops, grassland ecosystem and vegetation[3,7–9]. Thus, climate change has become one of the most severe challenges facing humankind. Attaching great importance to the change on different types of compound extreme events and doing research on it is the key to prevent and mitigate natural disasters and ensure the economic development and human happiness.

Since the Intergovernmental Panel on Climate Change Special Report on Climate Extremes (IPCC SREX) first explicitly proposed the conception of compound extreme event in 2012[10], the definition of compound extreme event has been continuously enriching and expanding[3,11]. As for compound extreme high temperature and drought/rainy events (CHTDE and CHTRE), the quantitative identification methods can be classified into three categories[11–13]. One category is that the concurrent extremes of different variables should be greater than or less than their specified extreme thresholds[14–16]. Another category is to recognize the compound event based on empirical statistical models of meteorological indicators like compound drought and heat wave magnitude index[7,17–19]. The third category is to implement the

probability statistic indicator based on joint distributions of multiple single event indicators. In this category, the effects of dependence and interaction between multiple extreme driving factors and compound extreme events are investigated[13,20,21]. The Standardized Compound Event Indicator developed by Standardized Precipitation Index (SPI) and Standardized Temperature Index are good examples of this category[22]. However, most of these indicators are obtained based on data at monthly time scale, whereas the variation at daily time scale is smoothed out. In addition, the interaction between different time scales and physical meteorological element are not well considered and the extreme degree of the compound events are not well quantified at present[12,23].

Increasing attention has been paid to CHTDE in recently years. The IPCC AR6[3] report indicates that the occurrence probability of CHTDE has been increasing at the global scale since the 1950s, and the frequency and intensity of CHTDE have increased with high confidence. Wang *et al*.[24] investigated the spatiotemporal changes of CHTDE over global land using SPI and copula method. They demonstrated that the significant increase in the probability of CHTDE depends on the enhancement of negative correlation between temperature and SPI. In China, monthly CHTDE show an obvious increasing trend, which is evident in both the observations and numerical simulations, especially in Northeast China, where the occurrence probability of CHTDE has increased by 0.05 per decade[25–27]. In addition, the continuous and stable high pressure system anomaly is conducive to the formation of downdrafts and low-level thermal anomalies, which can effectively reduce cloud cover and increase solar radiation. As a result, CHTDE are intensified in China and display a daily variation feature[9,28,29]. However, few studies have focused on the regional characteristics of CHTDE and reproducibility in the simulations of CHTDE from the Coupled Model Intercomparison Project Phase 6 (CMIP6) on daily time scale. In addition, compared with the simulations of CHTDE by CMIP5, the performance and uncertainty range of CHTDE by CMIP6 have not been well understood.

Except for CHTDE, CHTRE also have important effects on the environment. When intensified extreme heavy precipitation events occur together with extreme high temperature events more frequently, a higher frequency of CHTRE can be found in both daytime and nighttime[15]. In addition, it is almost impossible for extreme precipitation events and extreme high temperature events to occur consecutively within a week in China before. However, it has become more likely that a once-in-50-year extreme precipitation event and an extreme high temperature event occur together within a week in recent decades[30]. However, our understanding of CHTRE is very limited, and little attention has been paid to the study of the severity of CHTRE based on the reliable observations and numerical model outputs at present.

In order to investigate the extent to which climate change is caused by anthropogenic activities, many studies on extreme events have been conducted and confirmed that anthropogenic activities, especially emissions of greenhouse gases, are the main reason for the increase in extreme temperature events, extreme precipitation events and drought events on both regional and global scales[4,31,32]. In recent years, human influence on compound extreme events has gradually attracted more attention. Some studies have found that anthropogenic activities are likely to influence the occurrence probability of global

CHTDE[25–27,33]. Specifically, under the background of global warming, the main driving factor for the increase of the frequency of CHTDE has changed from meteorological droughts in the 1930s to the observed warming trend in recent years[24,34]. However, the understanding of the changes in CHTDE and CHTRE influenced by anthropogenic activities and natural forcings in different regions of China is still less than sufficient.

The present study uses bivariate joint probability distribution method and multi-model results of CMIP6 to study changes in the severity of CHTDE and CHTRE in different subregions of China. Relative contributions of external forcings including anthropogenic activities and natural variability to the changes are also explored.

Results

Observed changes in CHTDE and CHTRE

In this study, the combined probability of the frequency and duration of simultaneously occurred high temperature and drought (rainy) events are considered and the severity of the compound event (see Methods) is quantified. Here, a smaller indexes of CHTDE and CHTRE (CHTDEI/CHTREI) represent a more violent and severe CHTDE/CHTRE. Therefore, a downward trend of CHTDEI/CHTREI indicates an increasing trend in the severity of CHTDE/CHTRE, and vice versa. To determine the optimal fitting copulas for calculating multivariate joint distribution, three criteria are used to compare the performance of different copulas[35]. According to the results, the CHTDEI and CHTREI based on the Clayton and Gumbel are shown in Fig. 1 (see Methods).

Specifically, the observed CHTDEI in Northwest China (NWC), Northeast China (NEC), the Tibetan Plateau (TP) and coastal region of south China (SC) exhibits a statistically significant (at the 95% confidence level) decreasing trend of about 0.04 to 0.1 per decade from 1961 to 2014 (Fig. 1a). This means that the severity of CHTDE is increasing significantly during summer in most areas of China except for eastern China (EC). In contrast, the CHTREI displays a significant decreasing trend of about 0.02 to 0.1 per decade in the north of TP and south of NWC (Fig. 1b). The intensified severity of CHTRE in NWC under the background of increasing warming and humidification deserves more attention[36]. In addition, there is a decreasing trend of about 0.02 to 0.06 only in the northern part of NEC. Moreover, the spatial patterns of observed trends in the severity of CHTDE and CHTRE found in this paper are basically similar to the results of previous research on the climatology of the frequency of CHTDE and CHTRE[18,37], which indicate that the severity of CHTDE and CHTRE would increase significantly in areas with higher frequency of CHTDE and CHTRE.

Note that the regional differences in CHTDE and CHTRE are significant and the driving factors in different regions may be different. Thus, the present study focuses on the CHTDE and CHTRE in five subregions of China, which are the NWC, TP, NEC, EC and SC regions shown in Fig. 1.

Model performance

In general, the accuracy of detection and attribution results depends on the performance of a large number of climate models[38]. To identify those models that can yield reasonable simulations, the capabilities of the 12 CMIP6 models for the simulation of climatological spatial pattern and temporal evolution of temperature and precipitation in China are evaluated based on the Taylor analysis (see Methods). A good model simulation should have three characteristics, i.e., the standard deviation and correlation are close to unit and the root mean square error (RMSE) is close to zero [39].

As shown in Fig. 2a and 2b, most models can reproduce the climatological spatial pattern of mean temperature and total precipitation in the summers of 1961–2014. Comparative analysis indicates that, although the spatial correlation coefficients between the simulations of the 12 models and observations are greater than 0.8 and the RMSEs of the model simulations are less than 0.5, the performance of IPSL-CM6A-LR is relatively poor on the simulation of mean temperature variance since it overestimates the standard deviation of temperature. For the climatology of total precipitation, the spatial correlation coefficients between observed precipitation and simulations are around 0.8 and the RMSEs are smaller than 0.75 for all the 12 models except FGOALS-g3, which shows a relatively poor performance with a spatial correlation coefficient of 0.53 and a RMSE of 0.77 (Fig. 2b). Looking at differences in total precipitation between the simulations of CMIP6 models and observations, it can be found that the deviation mainly comes from obvious overestimation in the TP and underestimation in EC and SC (Fig. S2).

The deviations of mean temperature and total precipitation in summer is particularly large in the simulations. The standard deviations of temperature simulated by MIROC6, CNRM-CM6-1 and CanESM5 are quite different from that in the observations (Fig. 2c). For regional mean precipitation in China (Fig. 2d), the largest correlation coefficient between total precipitation simulated by the models and observations is smaller than 0.4. The correlation coefficients between observations and simulations of IPSL-CM6A-LR and FGOALS-g3 are even negative. Besides, precipitation displays a significant annual variability (Fig. S3), which can hardly be reproduced by climate models[40]. Note that the multi-model ensemble mean (MME) even further offsets the interannual variability between model simulations and leads a smaller standard deviation and a lower signal-to-noise ratio[41].

Overall, based on the evaluation of the performance of the 12 models, five models, i.e., MIROC6, CNRM-CM6-1, CanESM5, IPSL-CM6A-LR and FGOALS-g3, show relatively poor skills and their simulations are excluded in the study. The MME of the remaining seven models, which are ACCESS-CM2, BCC-CSM2-MR, CESM2, GFDL-ESM4, HadGEM3-GC31-LL, MRI-ESM2-0 and NorESM2-LM, are used for further analysis.

Detection and attribution

Based on the simulations of the seven CMIP6 models, the linear trends of CHTDEI and CHTREI under different forcings are obtained (Fig. 3). The result indicates that the observed intensification of CHTDE and CHTRE severity can be captured by CMIP6 models in most areas of China.

Specifically for CHTDE, the historical all forcing (hist-ALL) simulation displays a decreasing trend of CHTDEI that is broader than the observation, such as in EC and SC (Fig. 3a). Moreover, the MME response to hist-GHG is similar to its response to the hist-ANT, which is obtained by subtracting the hist-NAT simulation from the hist-ALL simulation. The hist-ANT and hist-GHG simulations exhibit an intensifying severity of CHTDE (Fig. 3c, 3e). However, the spatial distribution of hist-AER is likely to offset the decreasing trend of CHTDEI in the TP, EC and SC (Fig. 3b) and thus alleviate the intensification of CHTDE. Note that the trend under hist-AER is opposite to the observation in NEC, which may be related to aerosol-radiation and aerosol-cloud interactions and the reduction of aerosol emissions[42,43]. The MME response to other historical anthropogenic forcings (hist-OA) including land use and ozone (Fig. 3f) is estimated by subtracting the response to hist-GHG and hist-NAT from hist-ALL[44]. The result is similar to hist-NAT in Fig. 3d and shows an insignificant trend over China.

In general, the external forcings have similar effects on CHTRE and CHTDE. These forcings may increase the severity of CHTRE under the hist-ALL (Fig. 3g), hist-GHG (Fig. 3i) and hist-ANT (Fig. 3k) all over the China. Additionally, the result based on the MME of hist-AER shows an increasing trend of CHTREI in the TP and eastern China and a decreasing trend in NWC, suggesting that aerosols are favorable for the intensification of the severity of CHTRE in NWC (Fig. 3h).

Furthermore, the observed and simulated trends of regional average CHTDEI and CHTREI based on the non-overlapping three-year-mean CHTDEI and CHTREI from 1961 to 2014 are calculated and displayed in Fig. 4. Obviously, the downward trends of CHTDEI and CHTREI are − 0.13 and − 0.07, respectively, indicating that the severity of observed CHTDE and CHTRE has significantly increased across China.

Under the hist-ALL, hist-GHG and hist-ANT, the trends of regional average CHTDEI is basically consistent with the observation over entire China (Fig. 4a). For the CHTDEI in NWC, TP and NEC, the observed downward trend and the simulated downward trend under hist-ALL, hist-GHG and hist-ANT both are significant at the 95% confidence level, which is in agreement with the linear trend of the spatial pattern. However, there is an upward trend of CHTDEI under hist-AER, indicating that aerosols reduce the severity of CHTDE especially in TP, EC and SC. In addition, it is worth noting that there exists a significant upward trend of severity of CHTDE under hist-OA in China, especially in TP. As for CHTREI (Fig. 4b), under the influence of hist-ALL, hist-ANT and hist-GHG, the trend of CHTREI is significant and the variation strength is much larger than the observation in all the subregions of China. Moreover, there are a significant increasing trend of severity of CHTRE under hist-AER in China, particularly in TP, EC and SC and a downward trend under hist-OA in TP.

Based on the above observations and external forcings of MME, the optimal fingerprinting method (see Note S2) is used to quantify the influence of external forcings on observed CHTDEI or CHTREI during 1961–2014. To examine relative contributions of anthropogenic activities and natural forcing and separate the hist-NAT and hist-ANT signals from each other[45], the two-single analysis, which regresses observed CHTDEI and/or CHTREI onto hist-ANT and hist-NAT simultaneously, is applied for further analysis. Moreover, the observed CHTDEI and/or CHTREI are regressed onto hist-AER, hist-GHG, hist-OA

and hist-NAT simultaneously by four-signal analysis to clarify the relative effects of various external anthropogenic forcings on the changes of CHTDE and CHTRE compared to the effects of natural forcing signals[46,47].

Figure 5a presents the scaling factors obtained by regressing the time series of observed CHTDEI anomalies onto the MME response to single forcing for the period of 1961–2014. Across China, the scaling factors for hist-ALL, hist-ANT, hist-GHG, hist-OA and hist-NAT are significantly greater than zero, suggesting that the effects of both the anthropogenic forcing and natural forcing on CHTDE can be detected in China. For different subregions, the best estimate of scaling factors in hist-ANT and hist-GHG are very close to unit, indicating the severity of CHTDE under anthropogenic external forcing especially under hist-GHG is in good agreement with the observed severity of CHTDE. Specifically, the hist-ANT can be detected in five subregions in China and the hist-GHG can be detected in most areas of China except EC. The hist-OA can be detected in TP and SC. Moreover, the scaling factor of hist-AER in TP and SC is negative, which is consistent with the spatial pattern of hist-AER trend. In addition to anthropogenic forcing, the scaling factors and 90% uncertainty ranges of hist-NAT in NWC, NEC and SC are greater than zero, but the uncertainty ranges are much larger than that under other forcings (Fig. 5a). It is worth noting that the uncertainty range of scaling factor in NWC includes unit, indicating that single-signal hist-NAT is the crucial factor for the severity of CHTDE in NWC. In conclusion, the impacts of anthropogenic and natural forcings on the severity of CHTDE in most areas of China, particularly in NWC, NEC and SC, can be detected. The hist-ANT, especially the hist-GHG, is an important forcing for the change in the severity of CHTDE in China. In contrast, the hist-AER can reduce the severity of CHTDE in China, and this effect is most obvious in TP and SC.

As for the scaling factors from two-signal (Fig. 5c) and four-signal analysis (Fig. 5e) of CHTDEI, the residual consistency test indicates that all the results have reached the 90% confidence level, suggesting that the null hypothesis of observed CHTDEI is equal to the models, and thus the multi-signal regression model fits the observed data well. It is clear that the signals of hist-ANT and hist-GHG can be regarded as main external forcings that lead to changes in the severity of CHTDE in China. Furthermore, the signals of hist-OA and hist-NAT can also be detected robustly in multiple-signal analysis, which may be different from previous studies[26,27]. When focusing on each individual subregion in China, the impact of hist-ANT can be separated from that of hist-NAT to dominate the severity of CHTDE in most areas of China except TP. The hist-GHG can be separated from other forcings to dominate the severity of CHTDE in TP and NWC. Moreover, the hist-NAT can also be separated from anthropogenic forcing in NWC, but the uncertainty range of scaling factor is very large. In general, the hist-ANT and hist-GHG are the primary causes for the increasing severity of CHTDE, and they can be separated from other forcings to dominate the severity of CHTDE in China. In addition, the hist-NAT also has a great effect on the increasing severity of CHTDE in NWC.

Similarly, Fig. 5b, 5d and 5f show the scaling factors of CHTREI from single-signal, two-signal and four-signal, respectively. Obviously, hist-ALL can be detected in most areas of China except SC. Across China, the 90% confidence interval of scaling factor under hist-NAT is greater than zero and includes unit,

suggesting that the severity of CHTRE can be largely attributed to hist-NAT (Fig. 5b). In addition, the hist-ANT and hist-GHG can be detected robustly. In terms of different subregions, changes in the severity of CHTRE in NWC and TP can be attributed to both hist-ANT and hist-NAT. The scaling factor of hist-GHG is greater than zero in TP and the uncertainty range of scaling factor includes unit in NWC and NEC (Fig. 5b), which means the hist-GHG can be detected in changes of the severity of CHTRE in TP and the intensifying CHTRE in NWC and NEC can be further attributed to hist-GHG. In particular, the effects of hist-OA and hist-AER with a negative scaling factor may offset each other for the change of severity of CHTRE in TP. Additionally, hist-AER has positive influences on CHTRE in NWC (Fig. 5b), which verifies the preliminary conclusion obtained from Fig. 3h. However, according to the single-signal case, the detected signals for hist-ALL, hist-ANT and hist-GHG have overestimated the observed change in CHTRE. Overall, both hist-ANT and hist-NAT are favorable for the increasing severity of CHTRE in China, particularly in TP and NWC, where the linear trend of CHTREI changed significantly.

Judging from the multi-signal results, only the hist-NAT can be separated from anthropogenic forcing in China. Both hist-ANT and hist-GHG can be separated from other forcings to dominate the increasing severity of CHTRE in NWC. The hist-ANT can dominate the increasing severity of CHTRE in TP. For NEC and EC, the signal of hist-NAT seems to be more consistent with observed CHTRE but the uncertainty is large. This may be related to the weak trend and obvious variability of observed CHTRE (Fig. S8). Although the signals of hist-GHG and hist-ANT on CHTRE can be detected robustly across China, the long-term changes in the severity of CHTRE are largely attributed to hist-NAT. Additionally, significant increasing linear trend of severity on CHTRE occurs in TP and NWC, while both hist-ANT and hist-NAT are the primary causes of CHTRE in mainland China.

According to the original time series of CHTDEI and CHTREI, the long-term trends under hist-ANT and hist-GHG are basically consistent with that of observations, and the series with hist-NAT are more consistent with the variability of observations (Fig. S4 and Fig. S5). To reduce the multi-time scale variation on CHTDEI and CHTREI that may affect detection and attribution and identify the main sources of long-term trend in the severity of CHTDE and CHTRE, the original time series of CHTDEI and CHTREI are decomposed into nonlinear trend and interannual-to-decadal variability by Ensemble Empirical Mode Decomposition (EEMD) method (see Methods).

According to the scaling factors of nonlinear trends of CHTDEI and CHTREI, it can be found that the 90% confidence interval of CHTDEI trend of hist-GHG and hist-ANT is significantly reduced compared with the original time series, indicating that the reliability of the results is improved. As expected, the nonlinear long-term trend of CHTREI with significantly decreasing trend after 1980s indeed is caused by hist-GHG and hist-ANT in most areas of China, particularly in TP, NEC and SC (Fig. S7). In addition, the hist-OA signal also can be detected in the long-term trend of CHTDE. For CHTREI, the signals of hist-ALL, hist-ANT and hist-GHG can only be detected from nonlinear long-term trend of CHTREI in most areas of China except SC. The scaling factor of hist-AER in China is negative, which suggests the offsetting role of hist-AER on the decreasing trend of CHTREI (Fig. S9).

To quantify the changes in the severity of CHTDE and CHTRE attributed to different external forcings, Fig. 6a shows the attributable linear change of CHTDEI from 1961 to 2014. Across China, the observed CHTDEI decreased by − 0.24 (−0.32 to − 0.16) during 1961–2014. The attributable change of hist-ANT to observed CHTDEI is − 0.24 (−0.33 to − 0.15) in China, which probably contributes 100% to the observed linear change of the severity of CHTDE. The contribution from hist-ANT is greater than 95% in different subregions. Meanwhile, the observed CHTDEI is estimated to decrease by − 0.19 (−0.32 to − 0.07) for hist-GHG and − 0.08 (−0.03 to − 0.13) for hist-OA in China. That means the contribution from hist-GHG is 80% for the linear change of the severity of CHTDE, while 33% of the change is from hist-OA. However, the attributable change calculated based on negative scaling factor is considered meaningless[48]. Thus, for the attributable change of hist-AER in TP and EC with a scaling factor excluded the negative is 0.15 (−0.01 to 0.38), indicating that hist-AER partially offsets the decline in CHTDEI by about 39%. Moreover, the reason why the attributable change of hist-NAT is not obvious is that the trend of hist-NAT is weak.

For CHTRE in Fig. 6b, the relative ratio of attributable change of CHTREI under different external forcings from 1961 to 2014 is basically similar with CHTDEI. The major decreases in CHTREI in TP and NWC are − 0.20 (−0.25 to − 0.14) and − 0.17 (−0.22 to − 0.12), respectively. The attributable linear changes of hist-GHG, hist-ANT and hist-ALL all exceed about 90% of the observed change of the CHTRE severity in China. CHTREI is estimated to decrease by − 0.13 (−0.19 to − 0.06) for hist-ANT, which accounts for 99% of the increasing severity of CHTRE across China. Specifically, CHTREI decreases by − 0.12 (−0.21 to − 0.04) for hist-GHG, − 0.02 (−0.04 to − 0.003) for hist-OA and − 0.01 (−0.02 to − 0.004) for hist-NAT, and they contribute to the increased severity of CHTRE by about 95%, 15%, and 8%, respectively. This illustrates that anthropogenic climate change is more important than natural climate change for the linear change of increasing severity of CHTRE across China. However, the linear change of hist-AER plays a role in reducing the severity of CHTDE, especially in TP and EC.

Discussion

In this paper, the indices that can represent both the occurrence frequency and the duration of CHTDE and CHTRE and characterize the severity of compound extreme events are established based on copula and relative threshold counting method. Furthermore, using temperature and precipitation simulated by CMIP6 models that have decent performance in China, detection and attribution analysis of the severity of CHTDE and CHTRE in the summers from 1961 to 2014 is carried out. The results indicate that the severity of CHTDE shows a significant increasing trend in most areas of China except EC. The hist-All, hist-ANT and hist-GHG can reproduce the observed trend of the CHTDE severity at the 95% confidence level. In addition, the severity of CHTRE has decreased in China, particularly in NWC, TP and NEC.

Further analysis by quantitative optimal fingerprinting method shows that the change in the CHTDE severity in China can be largely attributed to hist-ANT and especially hist-GHG. In addition, hist-GHG and hist-ANT can be separated from other external forcings to dominate the change of CHTDE across China, which produce more than 80% of the attributable contribution to observed CHTDE. In addition, the long-term trend of CHTRE under hist-OA can be successfully detected. On the contrary, hist-AER can partially

offset the increasing trend of the severity of CHTDE due to the greenhouse gases forcing, especially in TP and SC. In addition to anthropogenic forcings, the signal of hist-NAT can also be detected in China, especially in NWC and NEC. According to the EEMD decomposition, hist-NAT may be linked to the interannual-to-decadal variability of the severity of CHTDE in China.

In contrast, the change of the CHTRE severity is generally more influenced by hist-NAT. In China, the signal of hist-NAT with large uncertainty can be robustly detected in the change of CHTRE, particularly in TP, NEC and EC. In comparison, the influence of hist-ANT and hist-GHG can be detected robustly within a smaller uncertainty range across China. As for the NWC and TP, where the severity of CHTRE has an obvious long-term increasing trend, the trend can be attributed to the effect of hist-ANT. Moreover, the anthropogenic forcing contribute more than 90% for observed linear change of CHTRE severity.

In conclusion, anthropogenic activities are the primary factor that leads to the increased severity of CHTDE and CHTRE. However, the present study has some inadequacies. First, the external forcings are treated as linear superposition rather than nonlinear interaction in terms of attribution methods[49]. Second, it is obvious that there are some deviations in CMIP6 data, especially in the data of regional precipitation [40]. Therefore, it is necessary to adopt other effective methods and accurate regional climate model data to improve and verify the results. Third, the observed interannual-to-decadal variability of CHTREI is characterized by a 10-year quasi-periodic oscillation that is similar to CHTREI forced by hist-NAT, indicating that solar radiation and volcanic activities may influence interannual-to-decadal variability of the severity of CHTRE. This will be further studied in the future. Finally, the observations show that the severity of CHTDE and CHTRE in China is increasing, which is reflected by higher occurrence frequency and longer duration. Further analysis is necessary to explore the physical mechanisms behind CHTDE and CHTRE and their changes under different scenarios in the future.

Methods

Definitions of CHTDE index (CHTDEI) and CHTRE index (CHTREI)

To quantify the severity of compound events, CHTDEI and CHTREI are defined as combined probability of the frequency and duration of simultaneous occurrence of high temperature and drought (rainy) events. First, the concurrence of daily temperature greater than the 90th percentile and daily total precipitation greater than the 75th percentile (less than 25th percentile) in the summers (June, July and August) of 1961–2014 is defined as a potential CHTRE (CHTDE).

Second, the frequency (total number of potential CHTDE/CHTRE) and duration (maximum number of consecutive days in summer when potential CHTDE/CHTRE occurred) in each summer are taken as random variables *X* and *Y* with marginal distributions $F_X(x) = P(X \leq x)$ and $F_Y(y) = P(Y \leq y)$, respectively. The empirical Gringorten plotting formula is used to estimate marginal distributions of frequency and duration (See Text S2).

Finally, based on the frequency and duration of potential CHTDE and CHTRE, the bivariate copula $F(x,y) = P(X \le x, Y \le y) = C\left(F_X(x), F_Y(y); \theta\right)$ is used to construct the severity index $PI = P(X > x, Y > y) = 1 - F_X(x) - F_Y(y) + C\left(F_X(x), F_Y(y)\right)$ of compound extreme events. The three widely accepted Archimedean copulas are applied in this study. A smaller *PI* represents a smaller joint probability of more frequent (greater than *x*) and longer duration (greater than *y*), indicating that the potential CHTDE (CHTRE) is more severe. Here, the *x* and *y* represent the thresholds of *X* and *Y*. For convenience, the *PI* for CHTDE and CHTRE are called CHTDEI and CHTREI, respectively.

More detailed data and methods are given in the supplementary materials.

Declarations

DATA AVAILABILITY

The CMIP6 data are available at https://esgf-node.llnl.gov/search/cmip6/. The CN05.1 data are available at http://data.cma.cn/data/cdcindex/cid/00f8a0e6c590ac15.html.

CODE AVAILABILITY

The code to carry out the current analyses is available from the corresponding authors upon request.

ACKNOWLEDGEMENTS

This work was supported by the National Natural Science Foundation of China (grant 41991283), the National Key Research and Development Program of China (grant 2022YFF0801704), the National Natural Science Foundation of China (grant 42005015), and the Postgraduate Research & Practice Innovation Program of Jiangsu Province (grant KYCX22_1165).

AUTHOR CONTRIBUTIONS

B.S. and W.L. contributed to the conception of the study. W.L. and B.S. analyzed and interpreted the data. W.L. and B.S. wrote the manuscript. H.W., B.Z., H.L., R.X. and M.D. helped to edit the manuscript. X.L. and W.A. offered suggestions for revision.

COMPETING INTERESTS

The authors declare no competing interests.

References

1. Coumou, D. & Rahmstorf, S. A decade of weather extremes. Nat. Clim. Chang. **2**, 491–496 (2012).
2. Fischer, E. M., Sippel, S. & Knutti, R. Increasing probability of record-shattering climate extremes. Nat. Clim. Chang. **11**, 689–695 (2021).

3. IPCC. Climate change 2021. In: Masson-Delmotte, V. *et al.* (eds.). *The Physical Science Basis. Contribution of Working Group I to the Sixth Assessment Report of the Intergovernmental Panel on Climate Change. (*Cambridge, United Kingdom and New York. Cambridge University Press, 2021).
4. Zhou, B. & Qian, J. Changes of weather and climate extremes in the IPCC AR6 (in Chinese). Clim. Chang. Res. **17**, 713–718 (2021).
5. Liang, X. Extreme rainfall slows the global economy. Nature **601**, 193–194 (2022).
6. Cai, W. et al. The 2021 China report of the Lancet Countdown on health and climate change: seizing the window of opportunity. Lancet. Public. Health. **6**, e932–e947 (2021).
7. Mukherjee, S. & Mishra, A. K. Increase in compound drought and heatwaves in a warming world. Geophys. Res. Lett. **48**, 741–757 (2021).
8. Hao, Y. *et al*. Probabilistic assessments of the impacts of compound dry and hot events on global vegetation during growing seasons. Environ. Res. Lett. **16**, 074055 (2021).
9. Zhang, W. *et al*. Compound hydrometeorological extremes: drivers, mechanisms and methods. Front. Earth. Sci. **9**, 673495 (2021).
10. IPCC. Managing the risks of extreme events and disasters to advance climate change adaptation. Field, C. B. *et al*. (eds.). *A Special Report of Working Groups I and II of the Intergovernmental Panel on Climate Change*. (Cambridge, United Kingdom and New York. Cambridge University Press, 2012).
11. Zscheischler, J. *et al.* A typology of compound weather and climate events. Nat. Rev. Earth. Environ. **1**, 333–347 (2020).
12. Leonard, M. *et al.* A compound event framework for understanding extreme impacts. Wiley. Interdiscip. Rev. Clim. Change. **5**, 113–128 (2014).
13. Zscheischler, J. & Seneviratne S. I. Dependence of drivers affects risks associated with compound events. Sci. Adv. **3**, e1700263 (2017).
14. Bevacqua, E., Zappa, G. & Lehner, F. Zscheischler, J. Precipitation trends determine future occurrences of compound hot-dry events. Nat. Clim. Chang. **12**, 350–355 (2022).
15. Tencer, B., Weaver, A. & Zwiers, F. Joint occurrence of daily temperature and precipitation extreme events over Canada. J. Appl. Meteorol. Climatol. **53**, 2148–2162 (2014).
16. Xiao, X., Huang, D. & Yan, P. The climatic characteristics of compound extreme events (in Chinese). J. Meteorol. Sci. **40**, 744–751 (2020).
17. Wang, W., Zhang, Y., Guo, B., Ji, M. & Xu, Y. Compound droughts and heat waves over the Huai River Basin of China: From a perspective of the magnitude index. J. Hydrometeorol. **22**, 3107–3119 (2021).
18. Yu, R. & Zhai, P. More frequent and widespread persistent compound drought and heat event observed in China. Sci. Rep. **10**, 1–7 (2020).
19. Yu, R. & Zhai, P. Changes in compound drought and hot extreme events in summer over populated eastern China. Weather. Clim. Extremes. **30**, 100295 (2020).

20. Salvadori, G. & De Michele, C. Multivariate multiparameter extreme value models and return periods: A copula approach. Water. Resour. Res. **46**, W10501 (2010).
21. Sarhadi, A., Ausín, M. C., Wiper, M. P., Touma, D. & Diffenbaugh, N. S. Multidimensional risk in a nonstationary climate: Joint probability of increasingly severe warm and dry conditions. Sci. Adv. **4**, eaau3487 (2018).
22. Hao, Z., Hao, F., Singh, V. P. & Zhang, X. Statistical prediction of the severity of compound dry-hot events based on El Niño-Southern Oscillation. J. Hydrol. **572**, 243–50 (2019).
23. Yu, R. & Zhai, P. Advances in scientific understanding on compound extreme events (in Chinese). Trans. Atmos. Sci. **44**: 645–649 (2021).
24. Wang, R., Lü, G., Ning, L., Yuan, L. & Li, L. Likelihood of compound dry and hot extremes increased with stronger dependence during warm seasons. Atmos. Res. **260**, 105692 (2021).
25. Chen, H. & Sun, J. Anthropogenic warming has caused hot droughts more frequently in China. J. Hydrol. **544**, 306–318 (2017).
26. Li, H., Chen, H., Sun, B., Wang, H., & Sun, J. A detectable anthropogenic shift toward intensified summer hot drought events over northeastern China. Earth. Space. Sci. **7**, e2019EA000836 (2020).
27. Li, W., Jiang, Z., Li, L. Z., Luo, J. J. & Zhai, P. Detection and attribution of changes in summer compound hot and dry events over northeastern China with CMIP6 models. J. Meteorol. Res. **36**, 1–12 (2022).
28. Li, Y., Ding, Y. & Liu, Y. Mechanisms for regional compound hot extremes in the mid-lower reaches of the Yangtze River. Int. J. Climatol. **41**, 1292–1304 (2021).
29. Liu, Z. & Zhou, W. The 2019 autumn hot drought over the middle-lower reaches of the Yangtze River in China: Early propagation, process evolution, and concurrence. *J. Geophys. Res. Atmos.* **126**, e2020JD033742 (2021).
30. Chen, Y., Liao, Z., Shi, Y., Tian, Y. & Zhai, P. Detectable increases in sequential flood-heatwave events across China during 1961–2018. *Geophys. Res. Lett.* **48**, e2021GL092549 (2021).
31. Fischer, E. M. & Knutti, R. Anthropogenic contribution to global occurrence of heavy-precipitation and high-temperature extremes. Nat. Clim. Chang. **5**, 560–564 (2015).
32. Madakumbura, G. D., Thackeray, C. W., Norris, J., Goldenson, N. & Hall, A. Anthropogenic influence on extreme precipitation over global land areas seen in multiple observational datasets. Nat. Commun. **12**, 1–9 (2021).
33. Zscheischler, J. & Lehner, F. Attributing compound events to anthropogenic climate change. Bull. Amer. Meteor. Soc. **103**, E936–E953 (2022).
34. Alizadeh, M. R. *et al.* A century of observations reveals increasing likelihood of continental-scale compound dry-hot extremes. Sci. Adv. **6**, eaaz4571 (2020).
35. Sadegh, M., Ragno, E. & AghaKouchak, A. Multivariate Copula Analysis Toolbox (MvCAT): Describing dependence and underlying uncertainty using a Bayesian framework. Water. Resour. Res. **53**, 5166–5183 (2017).

36. Wei, K. & Wang, L. Reexamination of the aridity conditions in arid northwestern China for the last decade. J. Clim. **26**, 9594–9602 (2013).
37. Wu, X., Hao, Z., Hao, F. & Zhang, X. Variations of compound precipitation and temperature extremes in China during 1961–2014. Sci. Total. Environ. **663**, 731–737 (2019).
38. Sun, Y. *et al*. Recent progress in studies of climate change detection and attribution in the globe and China in the past 50 years (in Chinese). Adv. Clim. Chang. Res. **9**, 235–245 (2013).
39. Taylor, K. E. Summarizing multiple aspects of model performance in a single diagram. J. Geophys. Res. Atmos. **106**, 7183–7192 (2001).
40. Yazdandoost, F., Moradian, S., Izadi, A. & Aghakouchak, A. Evaluation of CMIP6 precipitation simulations across different climatic zones: Uncertainty and model intercomparison. Atmos. Res. **250**, 105369 (2021).
41. Zhao, T., Li, C. & Zuo, Z. Contributions of anthropogenic and external natural forcings to climate changes over China based on CMIP5 model simulations (in Chinese). Sci. China. Earth. Sci. **59**, 503–517 (2016).
42. Dong, B. *et al*. Abrupt summer warming and changes in temperature extremes over Northeast Asia since the mid-1990s: Drivers and physical processes. Adv. Atmos. Sci. **33**, 1005–1023 (2016).
43. Ye, J., Li, W., Li, L. & Zhang, F. “North drying and south wetting” summer precipitation trend over China and its potential linkage with aerosol loading. Atmos. Res. **125**, 12–9 (2013).
44. Najafi, M. R., Zwiers, F. W. & Gillett, N. P. Attribution of Arctic temperature change to greenhouse-gas and aerosol influences. Nat. Clim. Chang. **5**, 246–249 (2015).
45. Sun, Y. *et al*. Rapid increase in the risk of extreme summer heat in Eastern China. Nat. Clim. Chang. **4**, 1082–1085 (2014).
46. Ma, S. *et al*. Detectable anthropogenic shift toward heavy precipitation over eastern China. J. Clim. **30**, 1381–1396 (2017).
47. Sun Y *et al*. Understanding human influence on climate change in China. Natl. Sci. Rev. **9**, 128–43 (2022).
48. Min, S. K., Zhang, X., Zwiers, F. W. & Hegerl, G. C. Human contribution to more-intense precipitation extremes. Nature **470**, 378–381 (2011).
49. Allen, M. R. & Stott, P. A. Estimating signal amplitudes in optimal fingerprinting, Part I: Theory. Clim Dyn 2003; **21**: 477–491.

Figures

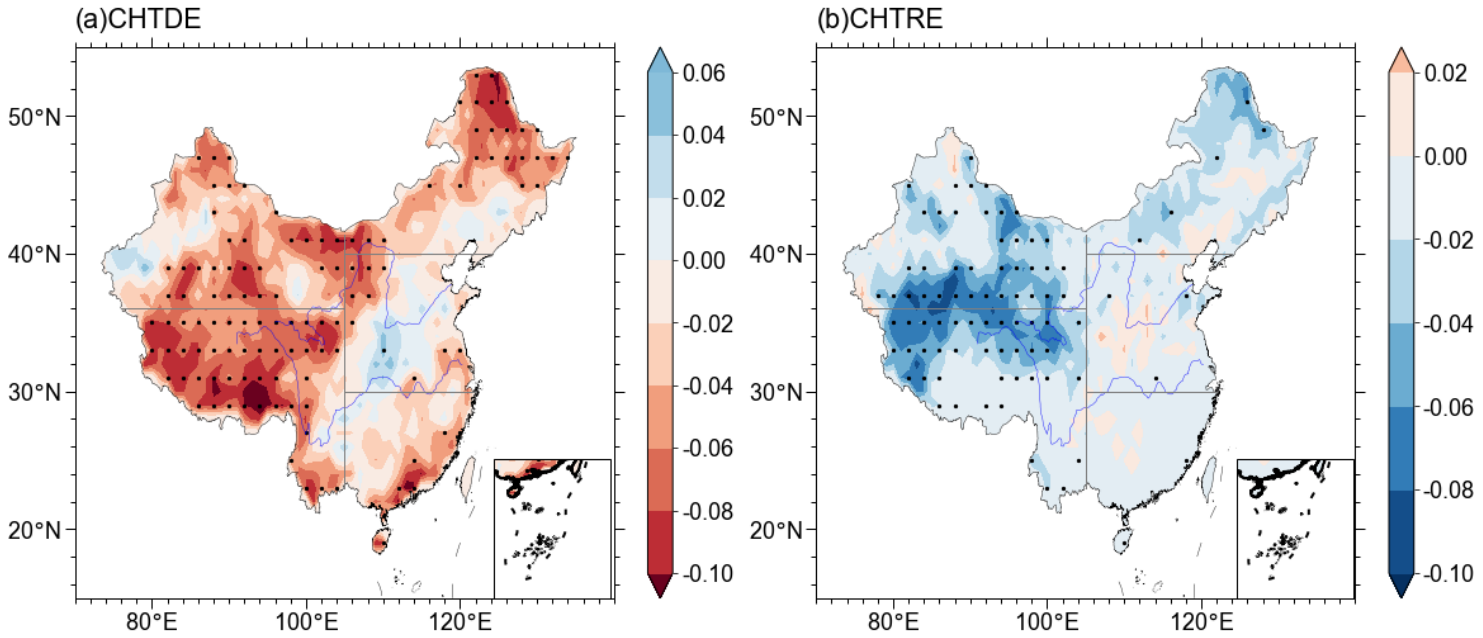

Figure 1

Linear trends of CHTDEI and CHTREI. Observed linear trends of (a) CHTDEI and (b) CHTREI based on CN05.1 in the summers from 1961 to 2014 (units: decade^{-1}) over China. Dotted area indicates the linear trend is significant at the 95% confidence level.

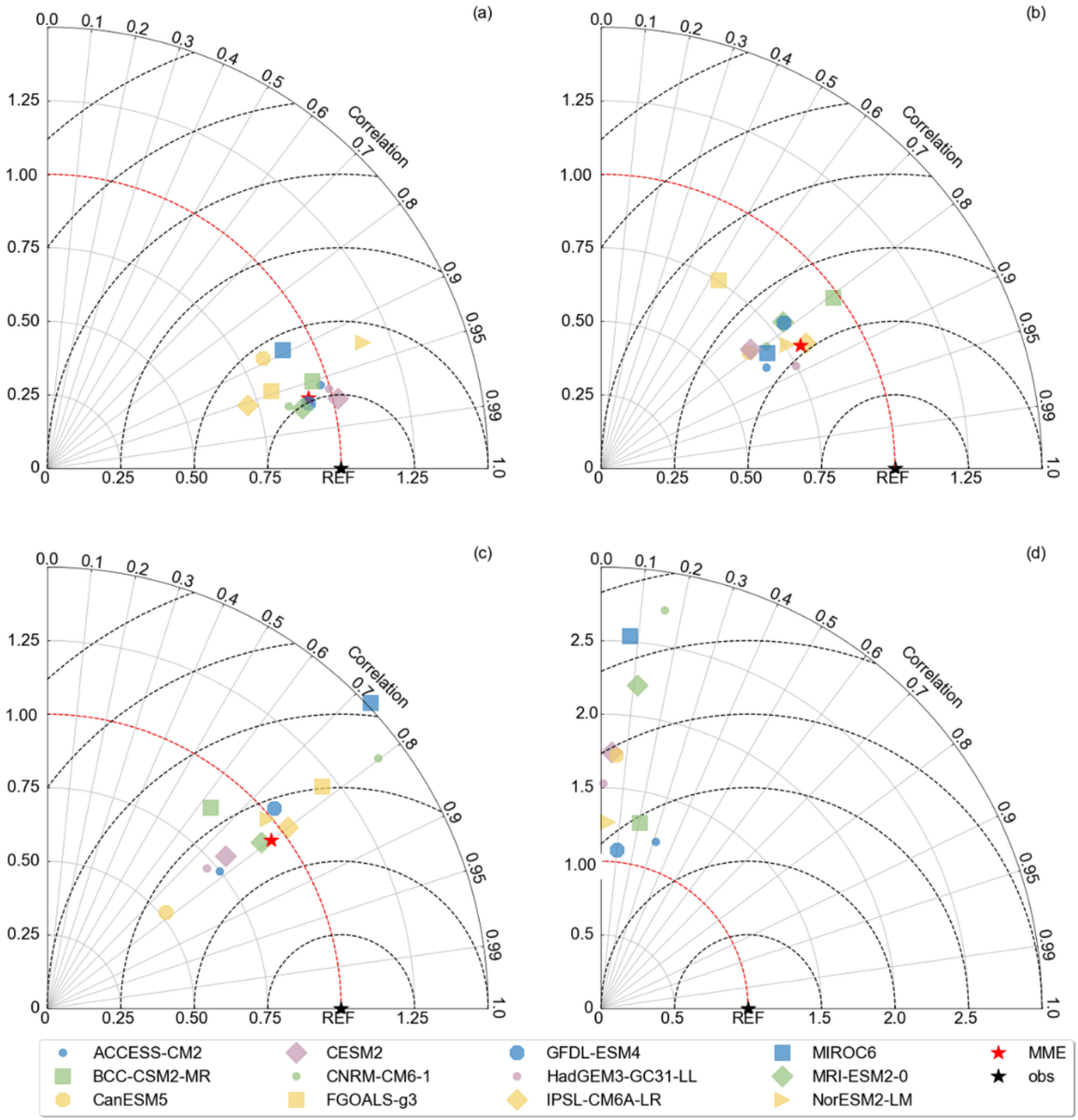

Figure 2

Taylor analysis of mean temperature and total precipitation. Taylor diagram showing the climatological spatial patterns of (a) mean temperature and (b) total precipitation and temporal evolution of (c) mean temperature and (d) total precipitation in summer over China. Symbols with different colors and shapes represent simulations of different models and MME as well as observations.

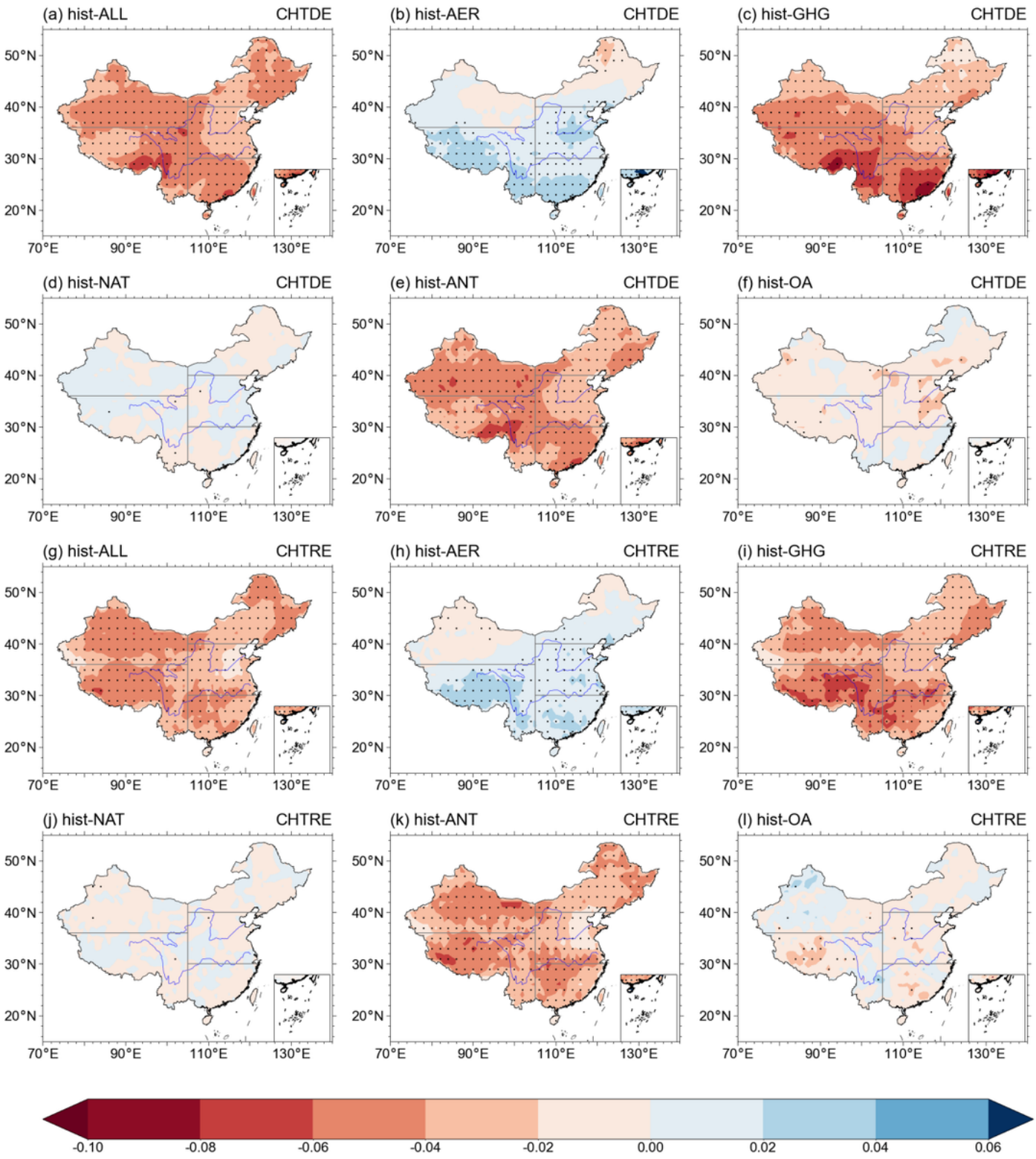

Figure 3

Linear trends of CHTDEI and CHTREI under different forcings. Linear trends of (a–f) CHTDEI and (g–l) CHTREI in response to different forcings (a and h for historical all forcing; b and h for historical anthropogenic aerosol forcing; c and i for historical greenhouse gases forcing; d and g for historical natural forcing; e and k for historical anthropogenic forcing; f and l for historical other anthropogenic

forcing) during the summers from 1961 to 2014 (units: decade^{-1}) over China. Dotted area indicates the linear trend is significant at the 95% confidence level.

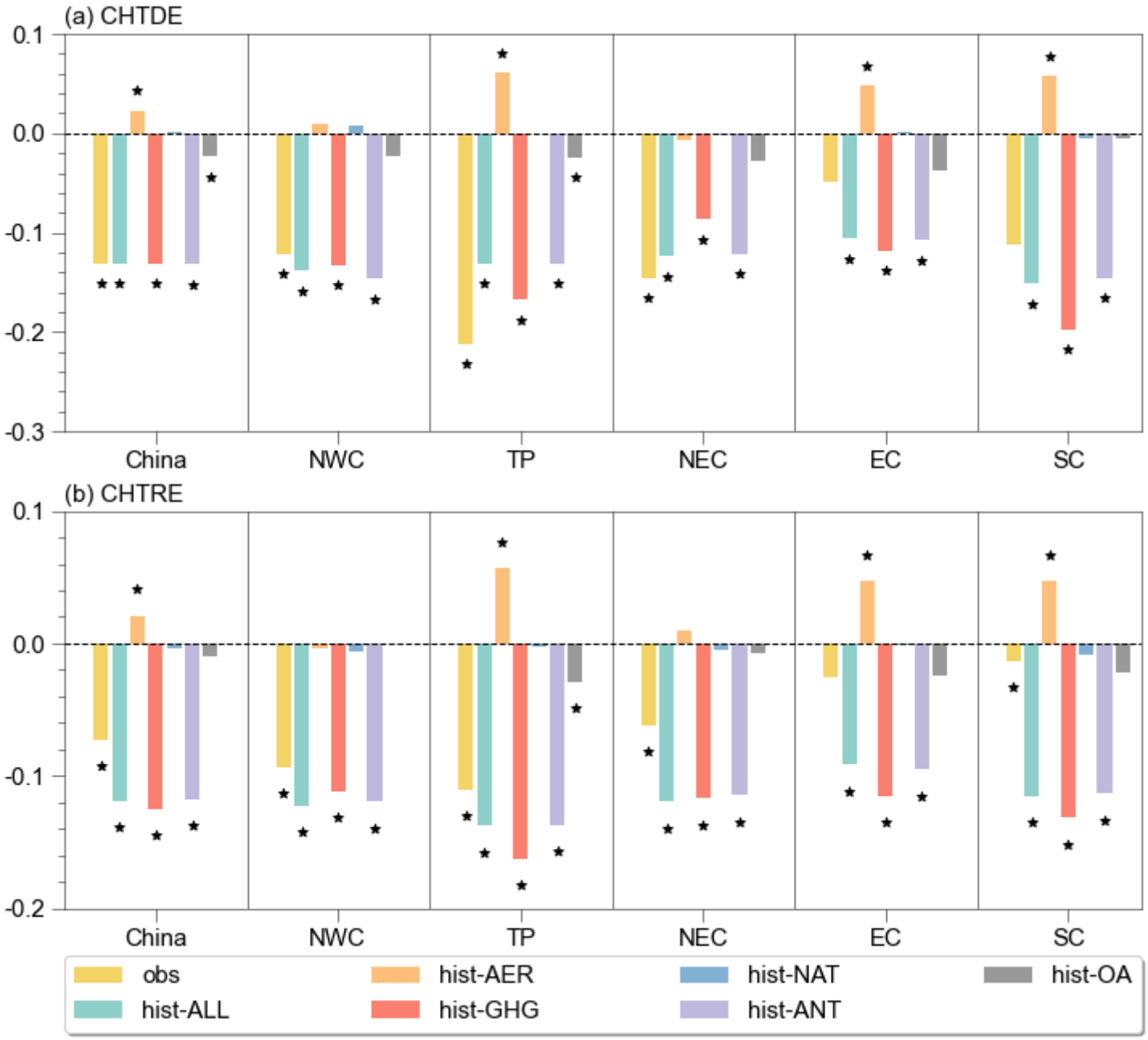

Figure 4

Linear trends of regional average CHTDEI and CHTREI from observations and simulations. Regional average trends for non-overlapping three-year-mean (a) CHTDEI and (b) CHTREI from observations and MME under external forcing across China and in different sub-regional of China (units: decade^{-1}). The asterisks denote the trend is significant at the 95% confidence level.

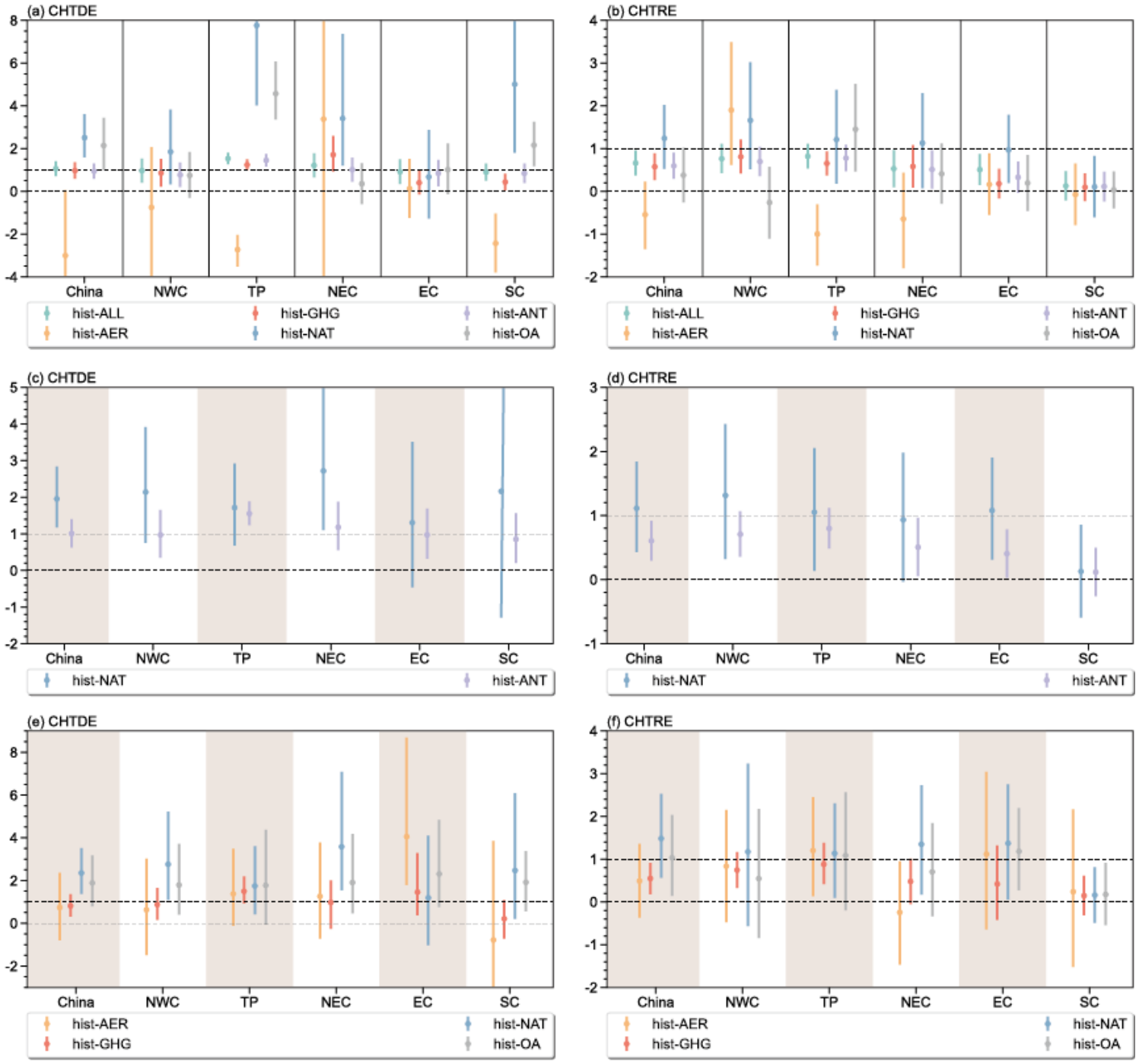

Figure 5

Detection and attribution analysis for the severity of CHTDE and CHTRE. Best estimates of the scaling factors (dots) and their 5–95% uncertainty ranges (error bars) from (a–b) single-signal (hist-ALL, hist-AER, hist-GHG, hist-NAT, hist-ANT and hist-OA), (c–d) two-signal (hist-NAT and hist-ANT) and (e–f) four-signal (hist-AER, hist-GHG, hist-NAT, and hist-OA) analysis for CHTDE and CHTRE in different subregions and across China. The two dashed lines parallel to the horizontal axis represent zero and unit, respectively.

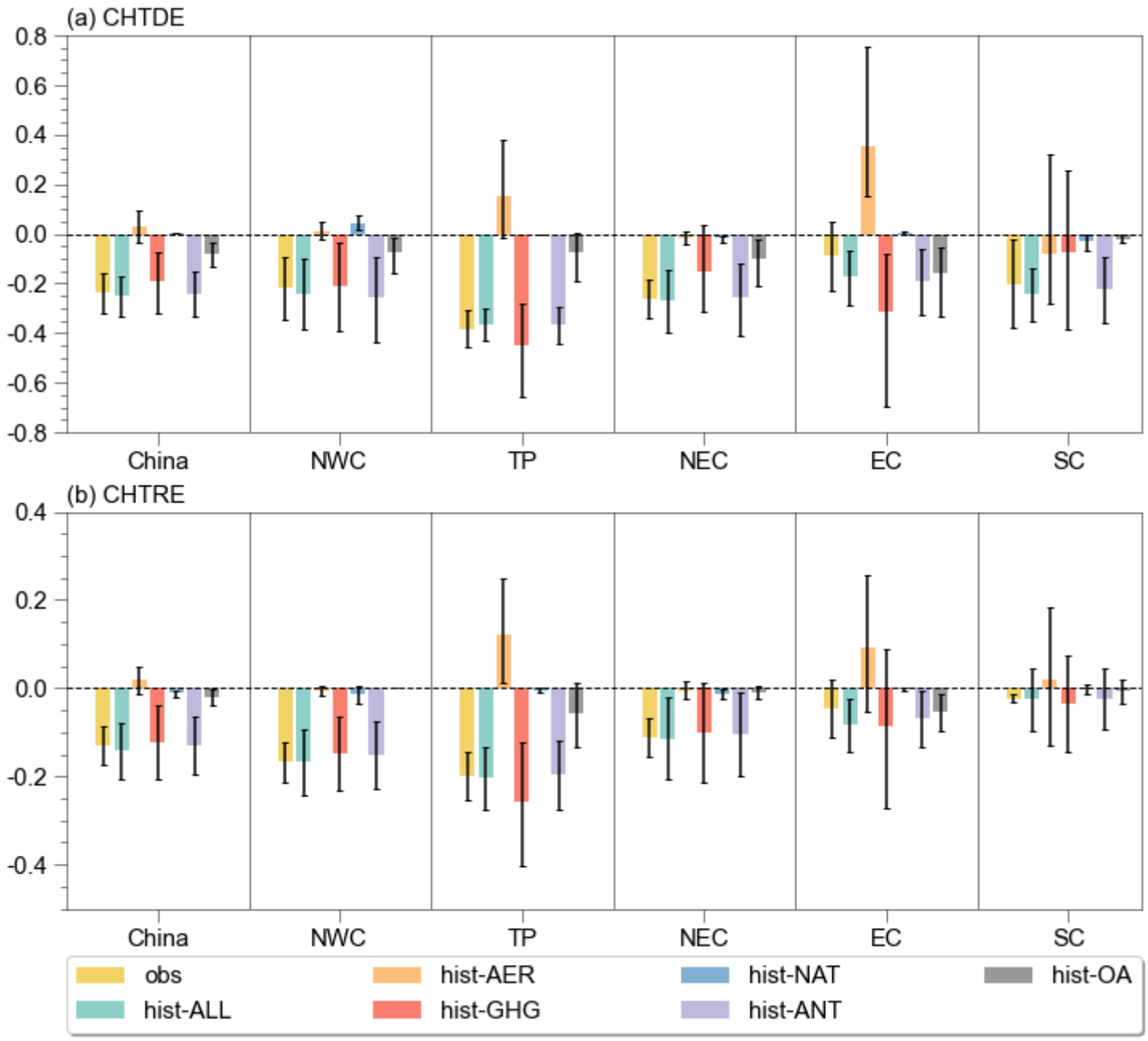

Figure 6

Attributed linear changes of CHTDE and CHTRE during 1961–2014. Estimates of observed linear changes in (a) CHTDE and (b) CHTRE and the corresponding total attributed linear changes in response to different external forcings based on the original change. The attributable linear changes are calculated by the trends for the MME of CHTDEI and CHTREI multiplied by the corresponding scaling factors (5%–95% margin of scaling factor) and then further multiplied by the periods of CHTDEI and CHTREI time series. Additionally, the observed changes of CHTDEI and CHTREI are estimated by the trend multiplied by the corresponding time period. The error bars indicate the 5–95% uncertainty range, while the 90% uncertainty range is calculated by the total least square method. The scaling factors used to constrain the attributable changes are derived by single-signal forcing for hist-ALL, two-signal forcing for hist-ANT and four-signal forcing for hist-AER, hist-GHG, hist-NAT and hist-OA.

Supplementary Files

This is a list of supplementary files associated with this preprint. Click to download.

- manuscript221211Supplementarydata.docx